Radiation Physics and Chemistry 202 (2023) 110539

Contents lists available at ScienceDirect

Radiation Physics and Chemistry

journal homepage: www.elsevier.com/locate/radphyschem

Coherent scattering cross sections of some rare earth compounds at small angles below 10° for 59.54 keV gamma rays

P.V. Thulasi [a,*], Antony Joseph [a], K.M. Varier [a], Somashekarappa H.M. [b], Vinayak Anand Kamat [c], Vishnu C.V. [a]

[a] Department of Physics, University of Calicut, Kerala 673635, India
[b] Centre for Application of Radioisotopes and Radiation Technology(CARRT), Mangalore University, Mangalagangotri, Karnataka 574199, India
[c] Department of Physics, Anjuman Arts, Science and Commerce College, Anjumanbad, Bhatkal 581320, India

ARTICLE INFO

Keywords:
Coherent scattering
Incoherent scattering
Rare earth oxides
Effective atomic number
Small angle scattering

ABSTRACT

The angle integrated total scattering cross sections of some rare earth oxides were determined experimentally for 59.54 keV gamma rays in the angular ranges of 0–4°, 0–6°, 0–8° and 0–10°. From the experimental total scattering cross sections, the corresponding angle integrated incoherent scattering cross sections obtained from ENDF library (based on the nonrelativistic Hartree–Fock form factor method) was subtracted to obtain the angle integrated coherent scattering cross sections. The angle integrated coherent scattering cross sections show good agreement with that determined from ENDF data. The effective atomic numbers of the selected rare earth oxides were extracted by applying the ratio of cross section method. The variation of angle integrated coherent scattering cross section with the effective atomic number of the selected compounds have been studied.

1. Introduction

Accurate values of coherent scattering cross sections of photons by materials are required in diverse fields such as radiation transport, attenuation, energy deposition, reactor shielding, industrial radiography, crystallography, plasma physics, astrophysics, medical diagnosis and imaging etc. (Kuruchu et al., 1998). It is also used extensively to obtain information on the structural properties of materials and macromolecules (Roy et al., 1999; Donativi et al., 2007). In the energy dispersive X-ray fluorescence technique using the fundamental parameter approach, the knowledge of both coherent and incoherent scattering cross sections are utilized to characterize the matrix of unknown samples (Simsek and Ertugrul, 2004). Fundamental parameter approach is a first principles calculation method of chemical element concentration from measured X-ray fluorescence spectra using fundamental parameters such as X-ray absorption coefficients, fluorescence yields, jump ratios, branching ratios, and the incident spectrum from the X-ray tube (Kawai et al., 2006). In condensed matter physics as well, coherent and incoherent scattering play a key role in the understanding of the excited states of many important systems (Singh et al., 2014). Coherent scattering is one of the major interaction processes of photons having energy below 1 MeV. Delbruck scattering, nuclear resonance scattering, Thomson scattering and Rayleigh scattering are the main processes which contribute to coherent scattering. Out of these, only Rayleigh scattering from bound electrons is the sole component of coherent scattering at low photon energies below 100 keV (Nayak et al., 1993; Varier, 2009). In Rayleigh scattering, the incident photons are scattered from bound electrons and in this process, the atoms of the scatterer are neither excited nor ionized. The scattered photons from different parts of the atomic clouds of electrons combine in phase to give the coherent scattering. The process mainly occurs for absorbers with large atomic numbers, where the electron binding energies influence the Compton effect (Kissel et al., 1980; Kissel, 2000).

Theoretically, mainly two methods have been developed for estimating the Rayleigh scattering cross sections: numerical partial wave calculation using second order S-matrix and Form Factor formalism (FF). In the form factor formalism, an extended charge distribution is considered, instead of a classical point charge, as assumed by Thomson (Chatterjee and Roy, 1998). Here, in FF, two approaches are there, relativistic and nonrelativistic, based on the ground state wavefunction used to derive the charge distribution. In 1936, Franz (1936) suggested an electron binding energy correction to FF and the resulting method is known as the Modified Form Factor (MFF) approach. Schaupp et al. (1983) in 1983 tabulated the modified relativistic atomic form factors (MFF) for elements with atomic number ranging from 1 to 100. Hubbell et al. (1975) had reported atomic form factors and incoherent scattering functions for elements with atomic number (Z) from 1 to 100. Here, the data values were obtained by following the nonrelativistic form factor

* Corresponding author.
E-mail address: thulasiabhilash@gmail.com (P.V. Thulasi).

https://doi.org/10.1016/j.radphyschem.2022.110539
Received 23 April 2022; Received in revised form 9 September 2022; Accepted 12 September 2022
Available online 15 September 2022

approach, with Hartree–Fock model for the charge distribution within the atom. Hubbell and Overbo (1979) had reported relativistic Hartree–Fock atomic form factors $F(x, Z)$, for all elements with Z from 1 to 100. In another study, Kahane (1998) had reported the relativistic Dirac Hartree–Fock photon incoherent scattering functions for elements with Z from 1 to 110, using the MFF approach. Chatterjee and Roy (1998) had reported the S-matrix differential elastic scattering cross sections for 14 photon energies in the range 50 keV–1500 keV, corresponding to 55 different scattering angles. The Evaluated Nuclear Data File (ENDF) store nuclear data from major evaluated libraries. The new ENDF/B-VIII.0 library (Brown et al., 2018), released in 2018, fully incorporates the new IAEA standard data and results from across the US and the international nuclear science community, over the last six years. The values of the atomic cross sections included in this library have been modified in recent updates of the nuclear data files (Midhun et al., 2019). Here, the newly recommended EPICS-2017 data, adapted in ENDF/B-VIII.0, have been used for the theoretical calculations of angle integrated coherent and incoherent scattering cross sections. In EPICS-2017, nonrelativistic form factor data (coherent) and nonrelativistic incoherent scattering functions of Hubbell et al. (1975) are included.

Many experimental investigations to determine the coherent scattering cross sections by different methods have been reported in literature (Basavaraju et al., 1994; Shahi et al., 1997; Bradley et al., 1999; Simsek and Ertugrul, 2004; Kane, 2005; Böke, 2011; Singh et al., 2012; Latha et al., 2012; Baek et al., 2012, 2014; Aldhuhaibat et al., 2020; Akkuş, 2020). İçelli and Erzeneoğlu (2002) have measured the ratio of differential scattering cross sections of coherent to Compton for 59.54 keV photons at 55° and 115° for Fe, Ni, Cu, Zn, Zr, Nb, Mo, Ag, Sn, Ta, Au and Pb targets, using Ge(Li) detector. They reported that the measured cross section ratio increases with increase in atomic number and are in good agreement with nonrelativistic and relativistic form factor theories. Singh et al. (2013) reported the coherent to incoherent scattering cross-section ratio of elements in the range $6 \leq Z \leq 82$, for 145 keV incident gamma photons at scattering angles of 50°, 70° and 90°. More recently, Akkuş et al. (2019) determined the variation of coherent to Compton scattering differential cross section ratios of some lanthanides at 59.54 keV. However, experimental studies are scarce for small angles below 10° and at low momentum transfer region, due to the difficulty in resolving the coherent scattered peak from the main peak, even by using high resolution detectors. Most of the scattering studies at small angles were done by shadow cone method (Roy et al., 1975; Kane et al., 1978; Ramanathan et al., 1979). In this method, the absolute source strength and other geometrical factors have to be measured, in addition to the scattered photon intensity. To overcome this difficulty, a new method had been suggested by Puttaswamy et al. (1984), using a simple geometrical setup, earlier used for gamma ray transmission studies. This method requires only the measurement of pure transmitted beam intensity in perfect narrow beam geometry setup and with small angle scattering contributions (Vinaykumar and Umesh, 2014a,b). Based on a subsequent study, Vinaykumar and Umesh (2016) have reported the angle integrated scattering cross section of 59.54 keV photons by elemental samples having atomic number in the region $13 \leq Z \leq 82$, employing this technique. But, so far no such studies are reported for rare earth oxides in the low momentum transfer region (0–10°). In the present study, we have determined the angle integrated total (coherent+ incoherent) scattering cross sections of oxides of rare earth elements in the lanthanide series, mainly $CeO_2, Dy_2O_3, Gd_2O_3, Nd_2O_3$ and Yb_2O_3 for 59.54 keV gamma rays in the angular ranges of 0–4°, 0–6°, 0–8° and 0–10°. From the total scattering cross sections, the corresponding angle integrated incoherent scattering cross sections obtained from ENDF library (based on the non-relativistic Hartree–Fock form factor method) is subtracted to obtain the angle integrated coherent scattering cross sections. The obtained angle integrated coherent scattering cross sections were compared with that determined from ENDF data. The effective atomic numbers of the selected rare earth oxides were extracted by applying the ratio of cross section method (Thulasi et al., 2021b). The variation of angle integrated coherent scattering cross section with the effective atomic number (Hine, 1952) of the selected compounds have been studied.

Oxides of lanthanides are extensively used for many applications in scientific, technological, medical, commercial and industrial fields (Niranjan et al., 2012). Cerium oxide is used in automobile exhaust catalysis as oxygen storage material. In electronic appliances, cerium dioxide replaces silicon dioxide, because of its ability to absorb and release oxygen under oxidizing and reducing conditions. Dysprosium oxide is used in cermets as nuclear reaction control rods. Gadolinium oxide is used in making metal oxide semiconductor field effect transistors. It is also used in garnets having microwave applications, compact discs, computer memory, nuclear marine propulsion systems as a burnable poison, an emergency shut-down measure in some nuclear reactors and as intravenous radiocontrast agents to enhance images in medical magnetic resonance imaging and in positron emission tomography (Singh et al., 2014). Neodymium oxide is used in ceramic capacitors, colour TV tubes, colouring glasses and in vacuum deposition. Ytterbium oxide is used in the manufacture of permanent magnet materials, glass, ceramic colouring agents and laser materials. In general, oxides of lanthanides are considered as better shielding materials to the exposure of gamma radiation. In this context, the studies on the interaction parameters of these compounds in the gamma radiation environment is appropriate.

2. Principle of the method

When perfect narrow beam geometry is ensured, no scattered radiations are assumed to fall on the detector and the transmitted intensity I_1 is given by Beer Lambert's law as,

$$I_1 = I_0 e^{-\mu t} \tag{1}$$

where I_o is the incident beam intensity, μ is the linear attenuation coefficient and t is the thickness of the absorber.

Now, if we allow some scattered radiations also to fall on the detector, it will reduce the value of the mass attenuation coefficient of the scatterer. Let I_2 be the intensity of transmitted plus scattered radiations, within a cone of forward acceptance angle θ_0. Then, $\Delta\mu$, the corresponding reduction in mass attenuation coefficient, can be expressed by the relation,

$$I_2 = I_0 e^{-(\mu-\Delta\mu)t} \tag{2}$$

From Eqs. (1) and (2), $\Delta\mu$, the contribution due to the scattered (coherent+incoherent) radiations is obtained as,

$$\Delta\mu = \frac{\ln\left(\frac{I_2}{I_1}\right)}{t} \tag{3}$$

The total scattering cross section $\Delta\sigma_{sca}$ from 0 to θ_0 in barn/molecule is then given by Vinaykumar and Umesh (2016),

$$\Delta\sigma_{sca} = \left(\frac{A}{0.60225}\right)\frac{\Delta\mu}{\rho} \tag{4}$$

where A is the molecular weight and ρ is the density of the scatterer.

$\Delta\sigma_{sca}$ constitute both the coherent and incoherent scattering cross sections within the angular range of 0 to θ_0, which is expressed as,

$$\Delta\sigma_{sca} = \int_o^{\theta_0} d\sigma_{coh} + \int_o^{\theta_0} d\sigma_{incoh} \tag{5}$$

The effective atomic numbers of the rare earth oxides are determined by the ratio of cross section method (Niranjan et al., 2012). In this method, first we deduce the atomic and electronic cross-sections from the experimental mass attenuation coefficients of the compounds (μ_c) and the mass attenuation coefficients of elements from the XCOM data (Berger and Hubbell, 1987). The effective atomic number is then obtained from the ratio of the atomic cross section (σ_a) to the electronic cross section (σ_e). Accordingly,

$$\sigma_a = \frac{\mu_c}{N_o \sum_i \frac{\omega_i}{A_i}} \tag{6}$$

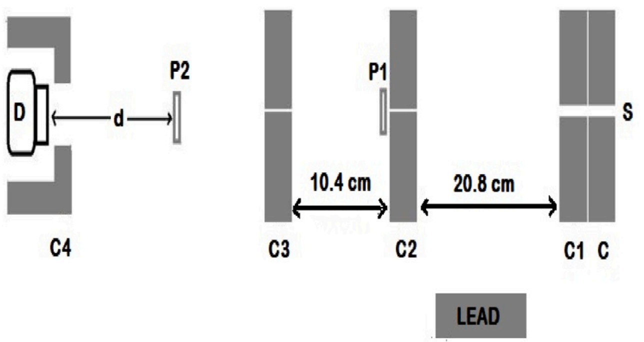

Fig. 1. The experimental setup. S is the source, D is the NaI(Tl) detector, C, C1, C2 C3, C4 are lead collimators and P1 and P2 are scatterer positions.

$$\sigma_e = \frac{1}{N_o} \sum_i \frac{\omega_i A_i \mu_i}{z_i} \quad (7)$$

In the above equations, N_o, ω_i, μ_i, A_i and z_i are the Avogadro number, weight fraction, mass attenuation coefficient, mass number and atomic number of the ith constituent element of the compound, respectively. Hence,

$$Z_{eff} = \frac{\sigma_a}{\sigma_e} \quad (8)$$

3. Experimental details

In the present study, an ^{241}Am source with activity of 11.1 GBq, emitting gamma rays of energy 59.54 keV was used. The geometry of the experimental set up is displayed in Fig. 1. The ^{241}Am source, in the form of a cylinder, had dimensions 10 mm in diameter and 6 mm in length. The photon beam emitted by the source was made fine narrow by the collimators C and C1. The beam is further shaped using the collimators C2 and C3, having narrow holes of 4 millimetres in diameter. A NaI(Tl) detector of crystal size 76 mm in length and 76 mm in diameter, with an integrally mount photomultiplier tube (Bicron make) and a universal MCA scintiSPEC, procured from Thermo Scientific, Germany, were used in this study. A collimator C4 with a hole of diameter 6 cm is kept in front of the detector window. The alignment of straight line geometry was ensured by optically checking using a laser beam. A Microsoft Windows based spectroscopic application software winTMCA32 was used for data acquisition and spectrum processing. Pellets of diameter 1 cm were prepared by using rare earth oxides in powdered form, having purity ≥ 99%. Before starting the experiment, the detector was calibrated with standard gamma ray sources. First, the scatterer was placed at the position P1 so that the perfect narrow beam geometry condition has been ensured. No scattered radiations were allowed to reach the detector and pure transmitted beam intensity I_1 was measured. Subsequently, the scatterer was placed at the position P2, so that the scattered radiations within a forward cone of 0–θ_0 were allowed to reach the detector along with the transmitted radiations. The corresponding intensity I_2 was determined, which contains the transmitted as well as the scattered photons within an angle θ_0. The angle of scattering θ_0 was taken as the half-angle of the cone of acceptance of the detector at the scatterer. The scattering angle in terms of the distance d between the detector and the scatterer can be written as,

$$\theta_0 = \tan^{-1}\left[\frac{3 \text{ cm}}{d \text{ (cm)}}\right] \quad (9)$$

By changing the distance d, the inscattering angle can be varied. By varying the position P2 and hence the distance d, the photon intensity I_2 (transmitted+scattered) for different angular ranges (0–4°, 0–6°, 0–8° and 0–10°) was measured. The spectra were acquired by placing each of the scatterer at the same position P1 and taking different positions for P2, in order to include the angular ranges 0–4°, 0–6°, 0–8° and 0–10°. The experiment was repeated 5 times at each position and the average value of I_2 was taken. The time for acquisition was decided in such a way that the counts under the photopeak was of the order of 10^5–10^6, so that the statistical error in percentage ($\frac{1}{\sqrt{counts}}\times 100$) estimated in each measurement is less than 0.5. The background counts were taken for the same interval of time by introducing a lead block of sufficient thickness in the path of the direct ray. From the background subtracted counts of I_1 and I_2, the total scattering cross section $\Delta\sigma_{sca}$ for each angular range of 0–θ_0 was determined. Suitable peak fitting routine was used to avoid multiple scattering (Singh et al., 2009). Sample impurity error correction was not applied because samples with purity greater than 99% was used here and impurities with high atomic numbers were absent in the samples. There was a built in provision in the MCA and the software for the dead time correction.

4. Calculation of the angle integrated scattering cross section

In the present study, the angle integrated coherent scattering cross section was obtained by subtracting the nonrelativistic Hartree–Fock (NRHF) values of the angle integrated incoherent scattering cross section from the total angle integrated scattering cross section, estimated from the experiment. Then the estimated angle integrated coherent scattering cross sections were compared with the corresponding ENDF values. This was done for all the selected compounds. The theoretical angle integrated coherent and incoherent scattering cross sections were obtained by numerical integration from 0 to θ_0. The integral for ENDF coherent scattering cross section is given as,

$$\sigma_{coh} = \int_o^{\theta_0} \frac{1}{2} r_o^2 (1+\cos^2\theta) \ \ |f(x,z)|^2 \ d\Omega \quad (10)$$

where f(x,z) is the form factor and r_0 is the classical electron radius and its value is taken as 2.818×10^{-15} m.

The integral for obtaining angle integrated incoherent (NRHF) scattering cross section is given as,

$$\sigma_{incoh} = \int_0^{\theta_0} \frac{d\sigma_{KN}(\theta)}{d\Omega} [S(x,Z)] \ \ d\Omega \quad (11)$$

where $\frac{d\sigma_{KN}(\theta)}{d\Omega}$ is the differential Klein–Nishina scattering cross section per electron, as per the well-known Klein–Nishina formula (Klein and Nishina, 1929) and $S(x,Z)$ is the incoherent scattering cross section. $d\Omega = 2\pi \sin\theta \, d\theta$ is the differential solid angle in steradian.

The angle integrated coherent and NRHF incoherent scattering cross sections for all the constituent elements were estimated and that for the compounds were determined by applying the mixture rule (Jackson and Hawkes, 1981). In the present method of estimating angle integrated coherent scattering cross sections of compounds, we have not included the interference effects that give rise to diffraction patterns (Savitzky et al., 2020)

5. Results and discussion

The total scattering cross section for the selected rare earth oxides were determined experimentally in the angular ranges 0–4°, 0–6°, 0–8° and 0–10° and the results are presented in Table 1. The angle integrated incoherent and coherent scattering cross sections were estimated by numerical integration of ENDF values and these values are also listed in Table 1. Here, in the present study, at 59.54 keV photon energy, for the selected angular ranges and for the selected samples, the incoherent scattering cross section is very low compared with the coherent contribution. This is in line with the report of Simsek and Ertugrul (2004). Yet, it is subtracted from the total cross section to extract the coherent cross sections and to ensure that the reported values contain only the coherent contribution. The relative dominance of coherent scattering over incoherent scattering can be explained based on the dependence

Table 1
Coherent scattering cross sections of 59.54 keV gamma rays for the selected rare earth oxides.

Sample	Distance d in cm	Angle in degrees	Experimental values of total scattering cross section (barn/molecule)	Incoherent scattering cross section from ENDF (barn/molecule)	Experimental values of coherent scattering cross section (barn/molecule)	Coherent scattering cross section from ENDF (barn/molecule)
CeO_2	42.90	0–4	2.61 ± 0.45	0.0058	2.60 ± 0.45	2.70
	28.54	0–6	5.14 ± 0.44	0.0201	5.12 ± 0.44	5.24
	21.35	0–8	7.89 ± 0.44	0.0471	7.84 ± 0.44	8.05
	17.01	0–10	10.91 ± 0.44	0.0898	10.82 ± 0.44	10.66
Yb_2O_3	42.90	0–4	4.64 ± 0.59	0.0057	4.63 ± 0.59	4.50
	28.54	0–6	9.32 ± 0.59	0.0201	9.30 ± 0.59	9.05
	21.35	0–8	14.88 ± 0.58	0.0481	14.83 ± 0.58	14.21
	17.01	0–10	20.18 ± 0.58	0.0931	20.09 ± 0.58	19.56
Nd_2O_3	42.90	0–4	2.96 ± 0.11	0.0059	2.95 ± 0.11	3.09
	28.54	0–6	6.17 ± 0.11	0.0205	6.15 ± 0.11	6.04
	21.35	0–8	9.68 ± 0.11	0.0482	9.63 ± 0.11	9.31
	17.01	0–10	13.2 ± 0.11	0.0921	13.11 ± 0.11	12.66
Dy_2O_3	42.90	0–4	3.86 ± 0.12	0.0058	3.85 ± 0.12	3.91
	28.54	0–6	7.48 ± 0.12	0.0203	7.46 ± 0.12	7.78
	21.35	0–8	11.9 ± 0.12	0.0483	11.85 ± 0.12	12.12
	17.01	0–10	17.18 ± 0.12	0.0892	17.10 ± 0.12	16.58
Gd_2O_3	42.90	0–4	3.48 ± 0.12	0.0059	3.47 ± 0.12	3.61
	28.54	0–6	6.96 ± 0.12	0.0206	6.94 ± 0.12	7.12
	21.35	0–8	10.89 ± 0.12	0.0487	10.84 ± 0.12	11.04
	17.01	0–10	14.94 ± 0.12	0.0935	14.85 ± 0.12	15.06

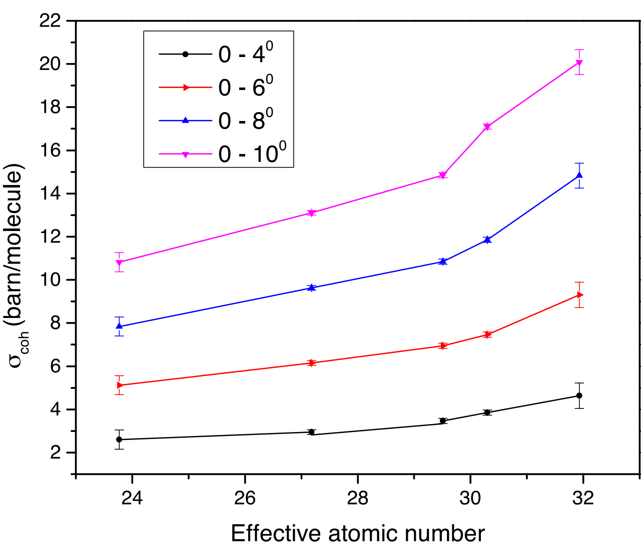

Fig. 2. Variation of the angle integrated cross section with effective atomic number.

of partial interaction cross sections of gamma rays for compounds on the atomic number of constituent elements, the energy of incident radiations and on the angle of scattering. Rayleigh scattering is the dominant interaction in high Z materials for photon energies below 100 keV (Kissel et al., 1980; Kissel, 2000); but incoherent scattering is the predominant interaction process in the medium energy range 100 keV - 10 MeV (Thulasi et al., 2021b). Also, for small scattering angles, coherent scattering is more dominant than incoherent scattering for low incident photon energies. The effective atomic number of the compounds were determined by the ratio of cross section method (Thulasi et al., 2021a). The experimentally determined angle integrated coherent scattering cross sections in specific angular ranges have been plotted against the effective atomic number of the rare earth oxides and the variation is shown in Fig. 2. This variation is similar to that reported by Vinaykumar and Umesh (2014b) in the case of lanthanides at 59.54 keV. Also this is in good agreement with the findings of Singh et al. (2013), who reported that the coherent to incoherent scattering cross-section ratio of elements, in the range $6 \leq Z \leq 82$, for 145 keV incident gamma photons at scattering angles of 50°, 70° and 90° increases with increase in atomic number. This variation is similar to the variation of Rayleigh scattering cross section with atomic number, for 662 keV gamma rays, as reported by (Varier, 2009). Only the statistical error in the experimental values are shown here, which are calculated using the formula (Akça and Erzeneoglu, 2014),

$$\delta(\Delta\sigma_{sca}) = K\sqrt{\left(\frac{\delta I_1}{I_1}\right)^2 + \left(\frac{\delta I_2}{I_2}\right)^2} \quad (12)$$

where $K = \frac{1}{\rho t}\left(\frac{A}{0.60225}\right)$

6. Conclusion

The angle integrated coherent scattering cross sections of the selected rare earth oxides were extracted by subtracting the corresponding incoherent contributions (based on NRHF model) from the experimentally determined total scattering cross sections, in four angular ranges, 0–4°, 0–6°, 0–8° and 0–10°. The obtained results agree well with the respective theoretical ENDF values. Also, the angle integrated coherent scattering cross sections in the specific angular ranges are found to increase with the effective atomic number of the rare earth oxides.

CRediT authorship contribution statement

P.V. Thulasi: Conception and design of study, Acquisition of data, Analysis and/or interpretation of data, Writing – original draft, Writing – review & editing. **Antony Joseph:** Conception and design of study, Acquisition of data, Analysis and/or interpretation of data, Writing – original draft, Writing – review & editing. **K.M. Varier:** Conception and design of study, Acquisition of data, Analysis and/or interpretation of data, Writing – original draft, Writing – review & editing. **Somashekarappa H.M.:** Conception and design of study, Acquisition of data, Analysis and/or interpretation of data, Writing – original draft, Writing – review & editing. **Vinayak Anand Kamat:** Conception and design of study, Acquisition of data, Analysis and/or interpretation of data, Writing – original draft, Writing – review & editing. **Vishnu C.V.:** Conception and design of study, Acquisition of data, Analysis and/or interpretation of data, Writing – original draft, Writing – review & editing.

Declaration of competing interest

The authors declare that they have no known competing financial interests or personal relationships that could have appeared to influence the work reported in this paper.

Data availability

We have taken data from Evaluated Nuclear Data File(ENDF) available in the International Atomic Energy Agency(IAEA) website for theoretical calculation of coherent scattering cross sections.

Acknowledgment

All authors approved the version of the manuscript to be published.

References

Akça, B., Erzeneoglu, S.Z., 2014. The mass attenuation coefficients, electronic, atomic, and molecular cross sections, effective atomic numbers, and electron densities for compounds of some biomedically important elements at 59.5 keV. Sci. Technol. Nucl. Install. 2014, 1–8. http://dx.doi.org/10.1155/2014/901465.

Akkuş, T., 2020. Measurement of coherent to compton scattering differential cross-section ratios of cadmium at different momentum transfer factors. Can. J. Phys. 98 (1), 102–106. http://dx.doi.org/10.1139/cjp-2019-0230.

Akkuş, T., Uğurlu, M., Demir, L., 2019. Variation of coherent to compton scattering differential cross-section ratios of some lanthanides with the external magnetic field at 59.54 keV. Results Phys. 13, 102265. http://dx.doi.org/10.1016/j.rinp.2019.102265.

Aldhuhaibat, M.J., Amana, M.S., Farhan, A.J., Jubier, N.J., 2020. Study of Cross Section Areas ratios for scattering interactions of Gamma photons in He, Fe, Fm, H_2O materials. In: IOP Conference Series: Materials Science and Engineering, Vol. 757, no. 1. IOP Publishing, 012013. http://dx.doi.org/10.1088/1757-899X/757/1/012013.

Baek, W., Bug, M., Rabus, H., 2014. Differential elastic electron-scattering cross sections of pyrimidine in the energy range between 20 eV and 1 keV. Phys. Rev. A 89 (6), 062716. http://dx.doi.org/10.1103/PhysRevA.89.062716.

Baek, W., Bug, M., Rabus, H., Gargioni, E., Grosswendt, B., 2012. Differential elastic and total electron scattering cross sections of tetrahydrofuran. Phys. Rev. A 86 (3), 032702. http://dx.doi.org/10.1103/PhysRevA.86.032702.

Basavaraju, G., Kane, P.P., Kissel, L.D., Pratt, R.H., 1994. Elastic scattering of 81 keV gamma rays. Phys. Rev. A 49, 3664–3672. http://dx.doi.org/10.1103/physreva.49.3664.

Berger, M.J., Hubbell, J.H., 1987. XCOM Photon Cross-Sections Database, Web Version 1.2.national Institute of Standards and Technology. Technical Report, http://dx.doi.org/10.2172/6016002.

Böke, A., 2011. Calculation of the total Rayleigh scattering cross sections of photons in the energy range of 30–50 keV for Nb and Mo elements. Radiat. Phys. Chem. 80 (5), 609–613. http://dx.doi.org/10.1016/j.radphyschem.2010.12.002.

Bradley, D., Gonçalves, O., Kane, P., 1999. Measurements of photon-atom elastic scattering cross sections in the photon energy range 1 keV to 4 MeV. Radiat. Phys. Chem. 56 (1), 125–150. http://dx.doi.org/10.1016/S0969-806X(99)00276-5.

Brown, D., Chadwick, M., Capote, R., Kahler, A., Trkov, A., Herman, M., Sonzogni, A., Danon, Y., Carlson, A., Dunn, M., Smith, D., Hale, G., Arbanas, G., Arcilla, R., Bates, C., Beck, B., Becker, B., Brown, F., Casperson, R., Conlin, J., Cullen, D., Descalle, M.-A., Firestone, R., Gaines, T., Guber, K., Hawari, A., Holmes, J., Johnson, T., Kawano, T., Kiedrowski, B., Koning, A., Kopecky, S., Leal, L., Lestone, J., Lubitz, C., Márquez Damián, J., Mattoon, C., McCutchan, E., Mughabghab, S., Navratil, P., Neudecker, D., Nobre, G., Noguere, G., Paris, M., Pigni, M., Plompen, A., Pritychenko, B., Pronyaev, V., Roubtsov, D., Rochman, D., Romano, P., Schillebeeckx, P., Simakov, S., Sin, M., Sirakov, I., Sleaford, B., Sobes, V., Soukhovitskii, E., Stetcu, I., Talou, P., Thompson, I., van der Marck, S., Welser-Sherrill, L., Wiarda, D., White, M., Wormald, J., Wright, R., Zerkle, M., Žerovnik, G., Zhu, Y., 2018. ENDF/B-VIII.0: the 8th major release of the nuclear reaction data library with CIELO-project cross sections, new standards and thermal scattering data. Nucl. Data Sheets 148, 1–142. http://dx.doi.org/10.1016/j.nds.2018.02.001.

Chatterjee, B.K., Roy, S.C., 1998. Tables of elastic scattering cross sections of photons in the energy range 50–1500 keV for all elements in the range $13 \leq Z \leq 104$. J. Phys. Chem. Ref. Data 27, 1011–1215. http://dx.doi.org/10.1063/1.556027.

Donativi, M., Quarta, S., Cesareo, R., Castellano, A., 2007. Rayleigh to compton ratio with monochromatic radiation from an X-ray tube preliminary results. Nucl. Instrum. Methods Phys. Res. B 264 (1), 189–193. http://dx.doi.org/10.1016/j.nimb.2007.09.017.

Franz, W., 1936. Rayleighsche streuung harter strahlung an schweren atomen. Z. Phys. 98, 314. http://dx.doi.org/10.1007/BF01331074.

Hine, P., 1952. The effective atomic numbers of materials for various gamma ray interactions. Phys. Rev 85, 725–737.

Hubbell, J.H., Overbo, I., 1979. Relativistic atomic form factors and photon coherent scattering cross sections. J. Phys. Chem. Ref. Data. 8, 69–106. http://dx.doi.org/10.1063/1.555593.

Hubbell, J.H., Veigele, W.J., Briggs, E.A., Brown, R.T., Cromer, D.T., Howerton, R.J., 1975. Atomic form factors, incoherent scattering functions, and photon scattering cross sections. J. Phys. Chern. Ref. Data. 4, 471–538. http://dx.doi.org/10.1063/1.555523.

İçelli, O., Erzeneoğlu, S., 2002. Experimental study on ratios of coherent scattering to compton scattering for elements with atomic numbers $26 \leq Z \leq 82$ in 59.5 keV for 55^o and 115^o. Spectrochim. Acta B: Atomic Spectroscopy 57 (8), 1317–1323. http://dx.doi.org/10.1016/S0584-8547(02)00050-2.

Jackson, D.F., Hawkes, D.J., 1981. X-ray attenuation coefficients of elements and mixtures. Phys. Rep. 70, 169–233. http://dx.doi.org/10.1016/0370-1573(81)90014-4.

Kahane, S., 1998. Relativistic Dirac hartree fock photon incoherent scattering functions. At. Data Nucl. Data Tables 68, 323–347. http://dx.doi.org/10.1006/adnd.1998.0770.

Kane, P., 2005. Elastic scattering of gamma rays and X-rays. Radiat. Phys. Chem. 74 (6), 402–410. http://dx.doi.org/10.1016/j.radphyschem.2005.08.004.

Kane, P.P., Basavaraju, G., Mahajani, J., Priyadarsini, A.K., 1978. Elastic and compton scattering of 1.17 and 1.33 MeV gamma rays through small angles. Nucl. Instr. Meth. 155, 467–474. http://dx.doi.org/10.1016/0029-554x(78)90531-1.

Kawai, J., Yamasaki, K., Tanaka, R., 2006. Fundamental parameter method in X-Ray fluorescence analysis. In: Encyclopedia of Analytical Chemistry: Applications, Theory and Instrumentation. Wiley Online Library, pp. 1–14. http://dx.doi.org/10.1002/9780470027318.a9666.

Kissel, L., 2000. RTAB: The Rayleigh scattering database. Radiat. Phys. Chem. 59 (2), 185–200. http://dx.doi.org/10.1016/S0969-806X(00)00290-5.

Kissel, L., Pratt, R., Roy, S., 1980. Rayleigh scattering by neutral atoms, 100 eV to 10 MeV. Phys. Rev. A 22 (5), 1970. http://dx.doi.org/10.1103/PhysRevA.22.1970.

Klein, O., Nishina, Y., 1929. Über die Streuung von Strahlung durch freie Elektronen nach der neuen relativistischen Quantendynamik von Dirac. Z. Phys. 52, 853–868. http://dx.doi.org/10.1007/bf01366453.

Kuruchu, Y., Erzeneoglu, S., Durak, R., Sahin, Y., 1998. Measurement of the compton and coherent scattering differential cross sections. Tr. J. Phys. 51, 45–48. http://dx.doi.org/10.1016/s0969-806x(97)00088-1.

Latha, P., Abdullah, K.K., Unnikrishnan, M.P., Varier, K.M., Babu, B.R.S., 2012. Differential scattering cross sections for elements with $13 \leq Z \leq 50$ using 59.54 keV gamma rays. Phys. Scr. 85, 035303. http://dx.doi.org/10.1088/0031-8949/85/03/035303.

Midhun, C.V., Musthafa, M.M., Akbar, S., Cyriac, S.L., Sajeev, S., Joseph, A., Jagadeesan, K.C., Suryanarayana, S.V., Ganesan, S., 2019. Spectroscopy of high-intensity bremsstrahlung using compton recoiled electrons. Nucl. Sci. Eng. 194, 207–212. http://dx.doi.org/10.1080/00295639.2019.1681210.

Nayak, N.G., Balakrishna, K.M., Siddappa, K., 1993. Experimental study on coherent scattering of 145.4 and 279.2 keV gamma rays by medium and heavy elements. J. Phys. B: At. Mol. Opt. Phya. 26, 4117–4126. http://dx.doi.org/10.1088/0953-4075/26/22/017.

Niranjan, R.S., Rudraswamy, B., Dhananjaya, N., 2012. Effective atomic number, electron density and kerma of gamma radiation for oxides of lanthanides. Pramana J. Phys. 78, 451–458. http://dx.doi.org/10.1007/s12043-011-0247-4.

Paternò, G., Cardarelli, P., Gambaccini, M., Taibi, A., 2020. Comprehensive data set to include interference effects in Monte Carlo models of X-ray coherent scattering inside biological tissues. Phys. Med. Biol. 65 (24), 245002. http://dx.doi.org/10.1088/1361-6560/aba7d2.

Puttaswamy, K., Gowda, M., Sanjeevaiah, B., 1984. A method for measuring integral scattering cross section of gamma rays for small angles. Nucl. Instrum. Methods Phys. Res. 224, 461–468. http://dx.doi.org/10.1016/0167-5087(84)90038-3.

Ramanathan, N., Kennett, T.J., Prestwich, W.V., 1979. An experimental investigation of small angle photon elastic scattering. Can. J. Phys. 57, 343–352. http://dx.doi.org/10.1139/p79-045.

Roy, S.C., Kissel, L., Pratt, R.H., 1999. Elastic scattering of photons. Radiat. Phys. Chem. 56 (1–2), 3–26. http://dx.doi.org/10.1016/S0969-806X(99)00286-8.

Roy, S.C., Nath, A., Ghose, A.M., 1975. Measurement of coherent scattering cross-sections of gamma rays at very low momentum transfer. Nucl. Instr. Meth. 131, 163–166. http://dx.doi.org/10.1016/0029-554x(75)90371-7.

Schaupp, D., Schumacher, M., Smend, F., Rullhusen, P., Hubbell, J.H., 1983. Small angle Rayleigh scattering of photons at high energies: Tabulations of relativistic HFS modified atomic form factors. J. Phys. Chem. Ref. Data 12 (3), 467–512. http://dx.doi.org/10.1063/1.555690.

Shahi, J.S., Puri, S., Mehta, D., Garg, M.L., Singh, N., Trehan, P.N., 1997. Elastic scattering of 22.1 keV photons by elements in the atomic region $12 \leq Z \leq 92$. Phys. Rev. A 55, 3557–3565.. http://dx.doi.org/10.1103/physreva.55.3557.

Simsek, O., Ertugrul, M., 2004. Angular dependence of coherent to incoherent scattering differential cross-section ratios for Zr, Nb and Mo elements. Radiat. Meas. 38, 271–276. http://dx.doi.org/10.1016/j.radmeas.2003.11.006.

Singh, M.P., Sharma, A., Singh, B., Sandhu, B.S., 2012. Experimental measurement of coherent to incoherent cross-section ratio of elements in the range $6 \leq Z \leq 82$ for 59.54 keV gamma photons. NISCAIR-CSIR, India, URL: http://nopr.niscair.res.in/handle/123456789/14310.

Singh, M.P., Sharma, A., Singh, B., Sandhu, B.S., 2013. An experimental study on cross section ratio of coherent to incoherent scattering for 145 keV incident gamma photons. Radiat. Meas. 59, 30–36. http://dx.doi.org/10.1016/j.radmeas.2013.09.003.

Singh, M.P., Sharma, A., Singh, B., Sandhu, B.S., 2014. Measurement of effective atomic number and Rayleigh-to-compton cross-section ratio for 145 keV gamma photons. J. Radioanal. Nucl. Chem. 302 (1), 187–194. http://dx.doi.org/10.1007/s10967-014-3282-z.

Singh, M.P., Singh, B., Sandhu, B.S., 2009. Investigations of multiple scattering of 320keV gamma rays a new technique for assigning effective atomic number to composite material. Phys. Scr. 79 (3), 035101. http://dx.doi.org/10.1088/0031-8949/79/03/035101.

Thulasi, P.V., Joseph, A., Varier, K.M., 2021a. Effective atomic number studies in coconut oil samples using 662 keV gamma rays. AIP Conf. Proc. http://dx.doi.org/10.1063/5.0058266.

Thulasi, P.V., Joseph, A., Varier, K.M., 2021b. Studies on partial and total photon interaction parameters in the energy range 1 keV–100 GeV of some synthetic polymers having medical applications. Radiat. Phys. Chem. 180, 109252. http://dx.doi.org/10.1016/j.radphyschem.2020.109252.

Varier, K.M., 2009. Nuclear Radiation Detection, Measurement and Analysis. Narosa publishing house, NewDelhi.

Vinaykumar, L., Umesh, T., 2014a. Coherent and incoherent scattering cross sections of some lead and sodium compounds at angles below 10^o for ^{241}Am Gamma rays. Phys. Res. Int. 2014, http://dx.doi.org/10.1155/2014/594767.

Vinaykumar, L., Umesh, T.K., 2014b. Coherent scattering cross sections of some lanthanides for ^{241}Am and ^{137}Cs gamma rays at low momentum transfer. Eur. Phys. J. D 68, http://dx.doi.org/10.1140/epjd/e2014-40678-5.

Vinaykumar, L., Umesh, T.K., 2016. Small angle scattering of 59.54 keV photons by elemental samples in the atomic number region $13 \leq Z \leq 82$. J. Radiat. Res. Appl. Sci. 9, 35–40. http://dx.doi.org/10.1016/j.jrras.2015.08.003.